

1A4-5

Delay Center of Broadband Antipodal Fermi Antenna and Its Application To Localization of Conducting Scatterer

Hiroyasu SATO, Kenji NAKANISHI, and Kunio SAWAYA
 Graduate School of Engineering, Tohoku University
 Aza-Aoba 05, Aramaki, Aobaku, Sendai, 980-8579, Japan
[†] E-mail: sahiro@ecei.tohoku.ac.jp

1 Introduction

Recently, many kinds of applications using EM pulse or broadband frequency range have been considered by many researchers so far. In the field of measurements, it is possible to realize high resolution pulse radar for the localization or the imaging of objects through walls, in concrete, under ground, concealed weapons inside the clothes etc by using broadband antenna. In order to realize the accurate localization of the scatterer located in wide angle region, it is important to clarify the position of phase center to obtain accurate position of scatterers. Also, the position of phase center should be located at the focal point to obtain an optimum coupling with lens for the application to the focal plane imaging. However, considering the radiation or the reception of pulse signals by using directive antenna, the phase center depends on not only the frequency but also the angle of the objects and it is considered not enough to study only the phase center.

In our previous work [1], the high gain antipodal Fermi antenna (APFA), which is one of the tapered slot antenna with the combination of antipodal feeding section and Fermi-Dirac taper section, has been proposed and applied to the through-wall imaging of metallic objects [2]. In this paper, an APFA designed for UWB band (3.1 GHz-10.6 GHz) is presented and the phase center of the APFA is investigated by FDTD analysis and the experiment. Also the delay pattern which is defined by the delay time of pulse peak and the delay center are obtained and applied to the localization of conducting scatterer by using two APFAs as monostatic radars.

2 Geometry

Fig. 1 shows the geometry of the APFA. The Fermi-Dirac taper is determined by $f(y) = a/(1 + e^{-b(y-c)})$, where a denotes the asymptotic value of the width of the taper for $y \rightarrow \infty$ and c denotes the y coordinate of the inflection point of the Fermi-Dirac function. Because of the relation of $f'(c) = ab/4$, b is related to the gradient at the inflection point c . Also there is a relation of $f(c) = a/2$ and $W = 2a$ when $b(L - c) \gg 1$. Dimensions of the APFA are shown in Fig. 1. FDTD analysis and the measurement were performed in the frequency range of 3 GHz to 10 GHz. In FDTD analysis, the cell size is $\Delta x=0.25$ mm, $\Delta y=0.5$ mm and $\Delta z=0.2$ mm, respectively. The number of time steps is 30,000 and the 8-layer PML was used. A gaussian pulse and the delta gap feed with 50Ω internal resistance were used for the excitation of the MSL.

3 Numerical and experimental investigations

The complex transmission coefficient S_{21} between two APFAs separated with a distance of 1.2 m in the opposite direction was measured. Frequency domain data measured by vector analyzer were converted into time domain data by the inverse Fourier transformation of complex S_{21} in the range from 3 GHz to 10 GHz with applying hanning window function. Generally, band limited pulse response becomes a burst pulse response, however, the envelope has been obtained by using Hilbert transformation. Fig. 2 shows the phase pattern at 6 GHz in E -plane (xy -plane) for cases when the APFA was rotated around points at $y=0$ and $y=L=200$ mm. Agreement

between measured and calculated values is obtained. By using the phase patterns for each frequency, the phase center was obtained by using the least mean square method in the range of $\phi = -30^\circ$ to 30° and is shown in Fig. 3. It is noted that the position of phase center p_y is located inside the antenna ($0 < p_y < L$) and varies with frequency. The variation of p_y in H -plane is larger than that of in E -plane.

As the phase center of the APFA varies with frequency, we introduce delay center. Fig. 4 shows the pulse response of the transmitting and the receiving APFAs when the transmitting APFA is rotated around a point at $y=L=200$ mm for $\phi=0^\circ$ and $\phi=36^\circ$ in both E -plane and H -plane. Decrease of pulse peak is observed with different delay time t_ϕ of pulse peak for the case of $\phi=36^\circ$. Difference of the delay time defined by $\Delta t_\phi = t_\phi - t_0$ were obtained as $+0.03$ ns in H -plane and -0.11 ns in E -plane, where t_0 is delay time of pulse peak when $\phi=0$. Fig. 5 (a), (b) show the the delay pattern in E -plane and H -plane defined by the delay time of pulse peak. In the case of E -plane, almost constant Δt_ϕ is obtained in the angle region of $|\phi| < 30^\circ$ when the APFA is rotated around a point at $y=0$. The delay center in E -plane obtained by using the delay pattern rotated at $y=L=200$ mm is $d_y^E=12$ mm. On the other hand, in the case of H -plane, almost constant Δt_ϕ is obtained when the APFA is rotated at $y=200$ mm. The delay center in H -plane obtained by using the delay pattern rotated at $y=0$ is $d_y^H=265$ mm. The values of delay center are also shown in Fig. 3.

Localization of metal cylinder were performed by using two APFAs as monostatic radars. The experimental configuration is shown in Fig. 6. A metal cylinder with radius of $a=20$ mm was located at $x_r=0-800$ mm, $y_r=800$ mm. Two APFAs were located along x axis separated with $l_x=300$ mm and complex S_{11} was measured in the frequency range of 3 GHz to 10 GHz. The delay time of scattered pulse responses obtained by IFT of complex S_{11} corresponds to the delay time from the scattering point (x_s, y_s) (shown in Fig. 7) and the effect of radius a was taken into account. The estimated point (x_e, y_e) is obtained by the cross point of two circles: $x_e^2 + (y_e - d_y)^2 = r_e^{(1)2}$ and $(x_e - l_x)^2 + (y_e - d_y)^2 = r_e^{(2)2}$ where d_y is the position of delay center $r_e^{(i)} = c(t_p^{(i)} - \tau) + (L - d_y)$, ($i = 1, 2$) where c is speed of light and τ is propagation time inside APFA. Fig. 8 and Fig. 9 show the estimation error by using E -plane APFAs and H -plane APFAs, respectively. The estimation error is defined by $\Delta R = \sqrt{(x_e - x_r)^2 + (y_e - y_r)^2}$ and $\Delta\phi = \left| \tan^{-1} \frac{y_e}{x_e} - \tan^{-1} \frac{y_r}{x_r} \right|$. In the case of E -plane APFAs, it is noted that ΔR and $\Delta\phi$ became small when $d_y=0$ ($\simeq d_y^E$). In the case of H -plane APFAs, ΔR and $\Delta\phi$ became small when $d_y=200$ mm ($\simeq d_y^H$). Because of the small error mentioned above, the validity of the delay center is confirmed.

4 Conclusion

The phase center and the delay center of an APFA designed for UWB band has been investigated and the localization of the conducting scatterer has been also performed. It has been found that the delay center is useful for the applications of pulse radar in case when the phase center depends on the frequency.

References

- [1] Y. Takagi, H. Sato, Y. Wagatsuma, K. Sawaya and K. Mizuno, "Study of high gain and broadband antipodal Fermi antenna with corrugation," International Symposium on Antennas and Propagation (ISAP2002), vol. 1, pp. 69-72, Sendai, Japan, 2004.
- [2] H. Sato, Y. Takagi, Y. Wagatsuma, K. Mizuno, and K. Sawaya, "Time Domain Characteristics of Broadband Antipodal Fermi Antenna And Its Application To Through-wall Imaging," International Symposium on Antennas and Propagation (ISAP2005), vol. 1, pp. 338-390, Seoul, Korea, 2005.

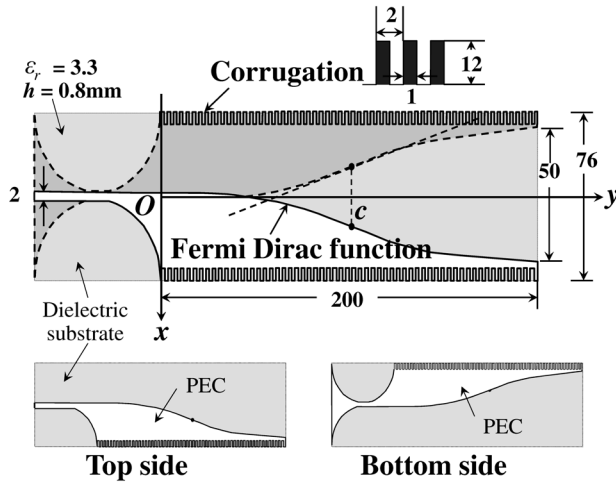


Figure 1: Geometry of APFA.

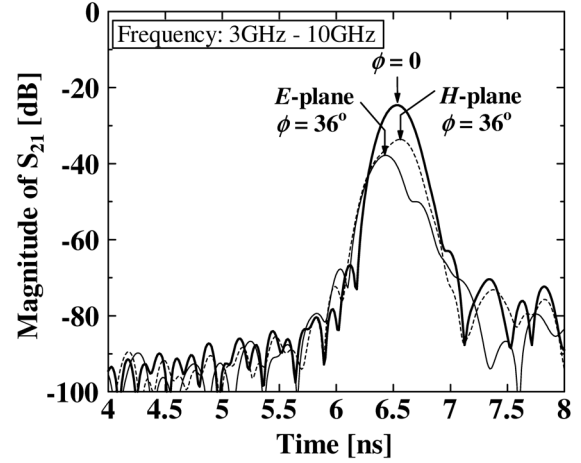


Figure 4: Pulse response of transmitting and receiving APFAs when transmitting APFA is rotated at $y=L=200$ mm.

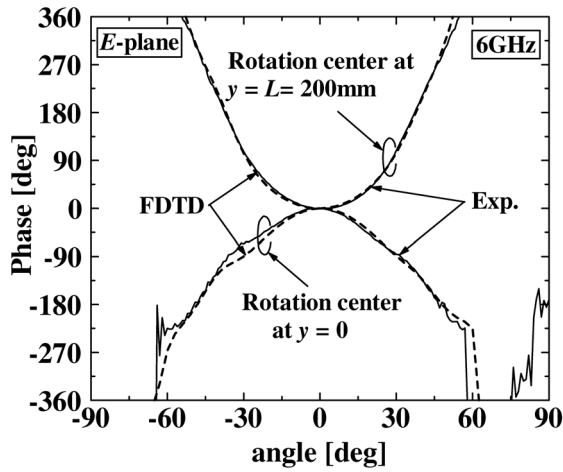
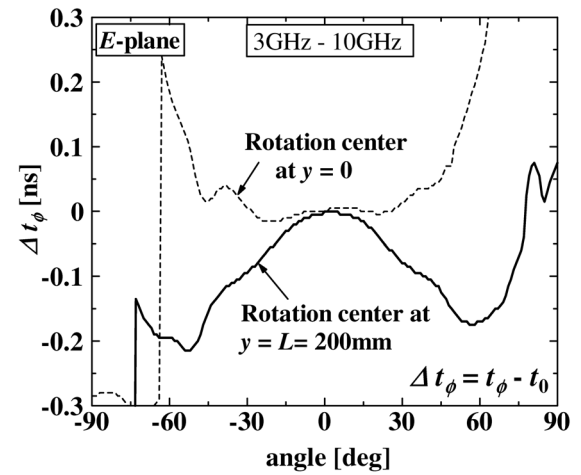


Figure 2: Phase pattern in E -plane (6 GHz, E_θ)



(a) E -plane

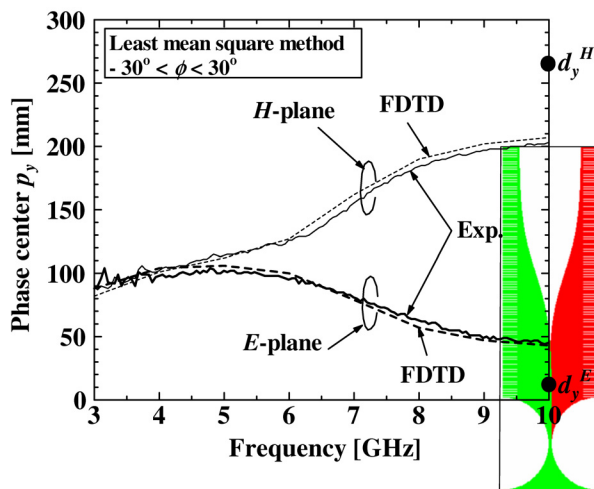
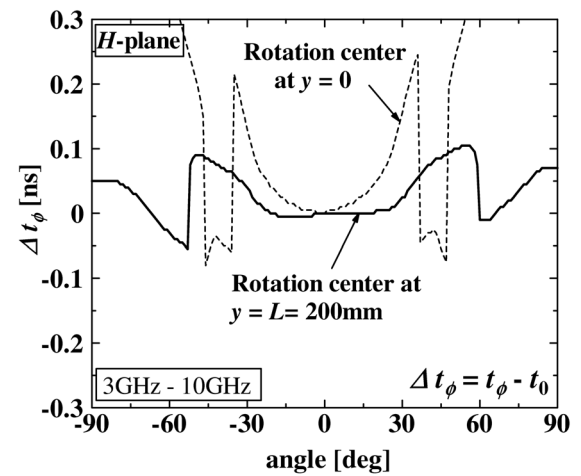


Figure 3: Phase center of APFA as a function of frequency.



(b) H -plane

Figure 5: Delay pattern obtained by delay time of pulse peak.

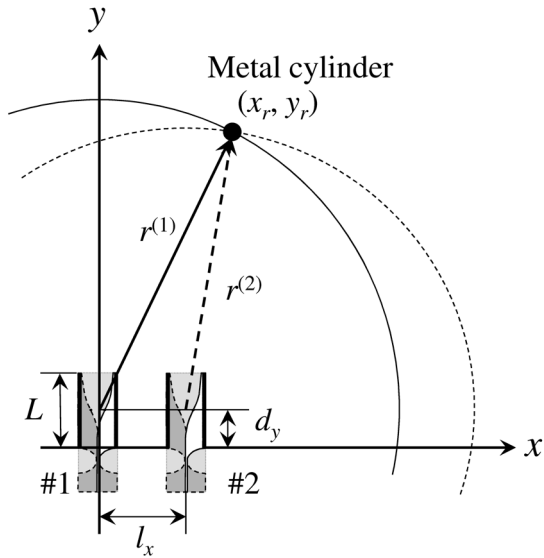


Figure 6: Configuration for estimation of metal cylinder (E -plane).

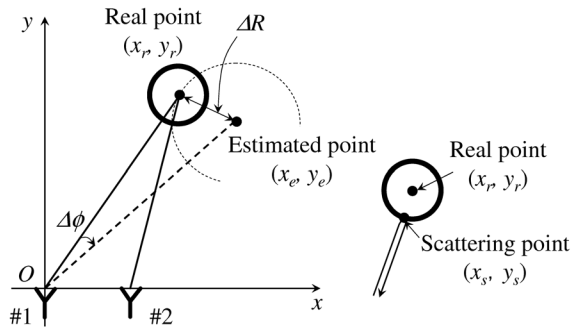


Figure 7: Definition of estimation error ΔR and $\Delta \phi$.

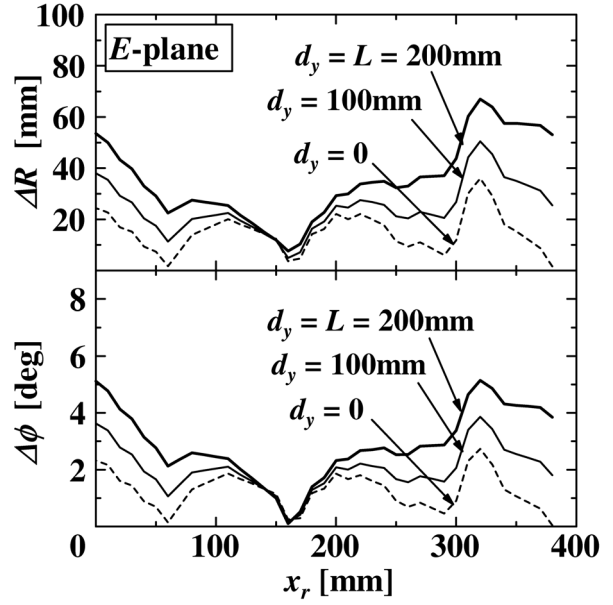


Figure 8: Estimation error as a function of real point x_r by using E -plane APFAs.

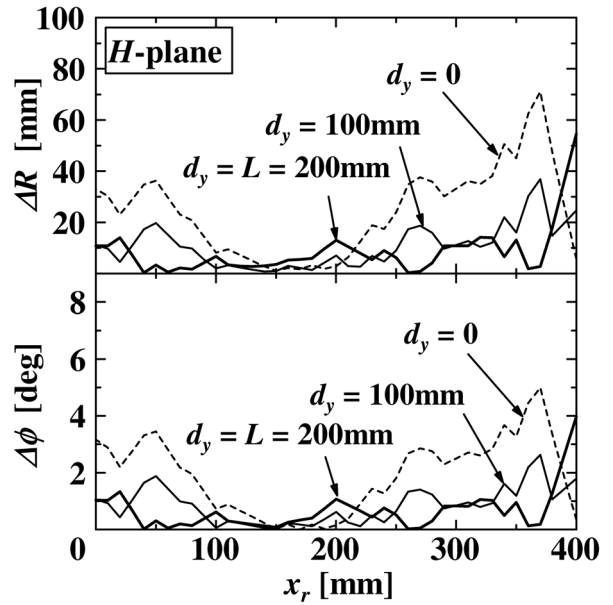


Figure 9: Estimation error as a function of real point x_r by using H -plane APFAs.